3-2012

Targeted Disruption of Toxoplasma gondii Serine Protease Inhibitor 1 Increases Bradyzoite Cyst Formation In Vitro and Parasite Tissue Burden in Mice

Viviana Pszenny
University of Pennsylvania

Paul H. Davis
University of Nebraska at Omaha, pdavis@unomaha.edu

Xing W. Zhou
Sun Yat-Sen University of Medical Sciences

Christopher A. Hunter
University of Pennsylvania

Vern B. Carruthers
University of Michigan - Ann Arbor

See next page for additional authors

Recommended Citation

Targeted Disruption of Toxoplasma gondii Serine Protease Inhibitor 1 Increases Bradyzoite Cyst Formation *In Vitro* and Parasite Tissue Burden in Mice

Viviana Pszenny
Departments of Biology, University of Pennsylvania, Philadelphia, Pennsylvania, USA

Paul H. Davis
Departments of Biology, University of Pennsylvania, Philadelphia, Pennsylvania, USA

Xing W. Zhou
Department of Biochemistry and Molecular Biology, Sun Yat-Sen University School of Medicine, Guangzhou, China

Christopher A. Hunter
Pathobiology, University of Pennsylvania, Philadelphia, Pennsylvania, USA

Vern B. Carruthers
Department of Microbiology and Immunology, University of Michigan Medical School, Ann Arbor, Michigan, USA

David S. Roos
Departments of Biology, University of Pennsylvania, Philadelphia, Pennsylvania, USA

Abstract: As an intracellular protozoan parasite, Toxoplasma gondii is likely to exploit proteases for host cell invasion, acquisition of nutrients, avoidance of host protective responses, escape from the parasitophorous vacuole, differentiation, and other activities. T. gondii serine protease inhibitor 1 (*Tg*PI1) is the most abundantly expressed protease inhibitor in parasite tachyzoites. We show here that alternative splicing produces two *Tg*PI1 isoforms, both of which are secreted via dense granules into the parasitophorous vacuole shortly after invasion, become progressively more abundant over the course of the infectious cycle, and can be detected in the infected host cell cytoplasm. To investigate *Tg*PI1 function, the endogenous genomic locus was disrupted in the RH strain background. Δ*Tg*PI1 parasites replicate normally as tachyzoites but exhibit increased bradyzoite gene transcription and labeling of vacuoles with Dolichos biflorus lectin under conditions promoting *in vitro* differentiation. The differentiation phenotype can be partially complemented by either *Tg*PI1 isoform. Mice infected with the Δ*Tg*PI1 mutant display ~3-fold-increased parasite burden in the spleen and liver, and this *in vivo* phenotype is also complemented by either *Tg*PI1 isoform. These results demonstrate that *Tg*PI1 influences both parasite virulence and bradyzoite differentiation, presumably by inhibiting parasite and/or host serine proteases.

Introduction

Parasitic life history strategies might be expected to balance host-pathogen interactions so that the competition between virulence factors and immune responses produces an equilibrium ensuring the survival of both the parasites and their hosts (2). Proteases have been shown to play an important role in pathogenesis in many viral, bacterial, and parasitic systems (20, 24, 33), and the regulation of protease activity is likely to be a critical aspect of pathogen biology (1). Serine protease inhibitors are commonly grouped into categories based on their primary sequences, structural motifs, and mechanisms of binding (28), and the Kazal, Kunitz, Serpin, and Smapin (small serine protein inhibitor) families have all been implicated in pathogen survival (21, 31, 32, 49, 51, 55, 56).

Protease inhibitors have been extensively characterized in metazoa but are absent from most of the protozoan taxa for which complete genomes are available (10). However, putative Kazal-type inhibitors have been identified in a subclass of apicomplexan parasites termed the Coccidia including Cryptosporidium (four genes), Neospora (at least two), and Toxoplasma (six); noncoccidial apicomplexan parasites (Plasmodium, Babesia, Theileria, etc.) show no evidence of any serine protease inhibitors. While the functions of coccidial Kazal-type protease inhibitors are not known, they have been hypothesized to protect parasites from proteolytic damage in the gut, suppress proteolytic activity during parasite replication, and counteract host proteases of the innate immune system (8, 39, 40, 44). Kazal-type protease inhibitors consist of one or more domains, each containing six conserved cysteines that form three intradomain disulfide bonds. Each domain displays an accessible surface loop containing a peptide bond called the reactive site, which specifically interacts with the active site of the target protease (44). All coccidian Kazal-type inhibitors appear to be “nonclassical” based on the short spacing between cysteines 1 and 2, a property that is thought to impart greater specificity for the target protease (22).

Biochemical studies have shown that Toxoplasma gondii serine protease inhibitor 1 (*Tg*PI1) inhibits a broad range of serine proteases (40), while *Tg*PI2 inhibits trypsin (39) and Neospora caninum PIS (*Nc*PIS) inhibits subtilisin (8, 41). All appear to traffic via the default “dense-granule” secretory pathway into the parasitophorous vacuole (PV), within which these obligate intracellular parasites replicate (26). Apicomplexan Kazal-type inhibitors could potentially target either parasite or host proteases, but their physiologically relevant targets remain unknown. To investigate the functions of these inhibitors, we genetically deleted *Tg*PI1, the dominant Kazal inhibitor in T. gondii (expressed at least 10-fold more highly than *Tg*PI2), which is present as two isoforms during all major stages of the parasite life cycle (tachyzoites, bradyzoites, and sporozoites). Δ*Tg*PI1 mutants exhibit altered differentiation and *in vivo* growth phenotypes that can be complemented by either *Tg*PI1 isoform.

Materials and Methods

Parasite and cell culture. All parasite strains were propagated as tachyzoites in human foreskin fibroblasts (HFF), as previously described (47). Wild-type RH, Prugniaud, and VEG strains were used as representatives of the type I, II, and III lineages defined by population genetic studies (23). Mutant parasites were constructed in the RHΔHXGPRT knockout background (16).

Western blotting, metabolic labeling, and immunoprecipitation. Parasites were harvested from infected HFF (in T25 flasks) by scraping and passage through a blunt 27-gauge needle, and the centrifuged pellets were resuspended in pH 7.6 phosphate-buffered saline (PBS) containing 5 mM $MgCl_2$, 0.5% Triton X-100, 100 U/ml DNase, and protease inhibitors (Sigma P8340). Proteins ($\sim 10^6$ tachyzoite equivalents per lane) were analyzed by SDS-PAGE on Novex bis-tris 4 to 12% gradient gels (Invitrogen) in parallel with prestained standards. After electrotransfer to nitrocellulose, the membranes were blocked in PBS containing 5% nonfat dry milk and 0.05% Tween 20 prior to adding rabbit anti-*Tg*PI1 (1:5,000) (44). After washing, the membranes were incubated with peroxidase-conjugated goat anti-rabbit antibody (Jackson ImmunoResearch) and visualized by chemiluminescence (GE Healthcare).

For metabolic labeling, confluent HFF monolayers in T175 flasks were infected with $\sim 4 \times 10^7$ tachyzoites 20 h before labeling for 15 min with [^{35}S]methionine/cysteine (50 mCi/ml). After washing, the cultures were chased for 0, 10, 25, or 60 min in unlabeled medium; harvested by scraping and centrifugation; passed 3 times through a 25-gauge needle; and solubilized in 1 ml RIPA buffer (50 mM Tris-HCl, pH 7.5, 1% Triton X-100, 0.5% sodium deoxycholate, 0.2% sodium dodecyl sulfate, 100 mM NaCl, 5 mM EDTA) containing 10 mg/ml RNase A, 20 mg/ml DNase I, and protease inhibitors. Samples were preincubated overnight at 4°C with protein G-Sepharose alone and centrifuged, and the supernatants were incubated for 1 h in rabbit anti-*Tg*PI1 antiserum, followed by the addition of protein G-Sepharose and further incubation for 1 h. The precipitated complexes were washed 4 times, boiled in electrophoresis buffer containing 10% SDS and 2% β-mercaptoethanol, separated by polyacrylamide gel electrophoresis, incubated in Amplify fluorographic enhancer (Amersham), dried on cellophane, and exposed to X-ray film.

MALDI mass spectrometry. Matrix-assisted laser desorption ionization—time of flight mass spectrometry (MALDI-TOF MS) was performed on a Voyager DE-STR (PerSeptive Biosystem) equipped with a 337-nm nitrogen laser. Unless otherwise specified, spectra were obtained in positive acquisition mode, and external peptides were used for calibration; the reported peptide masses are monoisotopic, while intact protein masses are average masses.

Parasites were cultivated in five T175 flasks until complete lysis of the host cell monolayer occurred, centrifuged, and passed through a 0.45-μm filter, and the filtrate (containing secreted *Tg*PI1) was incubated overnight with protein A-agarose beads (Bio-Rad) coupled to polyclonal rabbit anti-*Tg*PI1. After extensive washing with Tris, pH 8.0, bound protein was eluted in 100 mM glycine, pH 3.0, and protein-containing fractions (Bradford assay) were pooled and concentrated in a Centricon filter (Millipore). After electrophoresis on polyacrylamide gels and staining with copper, intact proteins were excised and extracted using standard methods (11): bands were sequentially incubated in 50 mM NH_4HCO_3 (10 min), followed by 50% acetonitrile, 200 mM NH_4HCO_3 (30 min, twice), and then high-performance liquid chromatography (HPLC) grade water; crushed with a pointed dental tool; covered with 20 μl of 10 mg/ml sinapinic acid (matrix) in 0.5% trifluoroacetic acid (TFA) in acetonitrile; and extracted by vortexing for 3 h at room temperature. Following extraction, the tubes were opened to evaporate the contents for ~20 min with vortexing until the matrix solution became slightly cloudy, and 1 μl supernatant was deposited onto the MALDI probe. After calibration with aldolase, spectra were acquired in linear mode (acceleration, 25 keV; 91% grid voltage; 1,000-ns delay; 100 laser shots per

spectrum), yielding an error of <10 atomic mass units. Peak masses were assigned based on the centroid at 50% height, and standard deviations were calculated based on at least three independent spectra per protein.

For peptide analysis, bands were excised, reduced by 1 h of incubation at 56°C in 50 mM dithiothreitol (in 100 mM NH_4CO_3), and alkylated by treatment for 45 min with 275 mM iodoacetamide (in 100 mM NH_4CO_3) in the dark. After in-gel digestion with 12.5 ng/μl trypsin in 50 mM NH_4HCO_3 and solvent extraction (50), the peptide mixtures were dried, dissolved in 2 μl 50% acetonitrile plus 0.3% TFA, mixed with saturated CHCA (α-cyano-4-hydroxycinnamic acid) matrix, and deposited on the MALDI MS target plate. Spectra were acquired in reflection mode with delayed extraction. Peptide mass fingerprints were used to search against the NCBI nonredundant database using MS-Fit (http://prospector.ucsf.edu) or FindPept (http://web.expasy.org/findpept/), based on a threshold mass deviation of 50 ppm.

Molecular genetic manipulations. Total parasite RNA was isolated from freshly harvested tachyzoites (RNAEasy; Qiagen), and 2 μg purified RNA was subjected to reverse transcription (RT)-PCR (60 min of reverse transcription at 42°C using Moloney murine leukemia virus reverse transcriptase [Promega]) amplification using Expand High Fidelity PCR (Roche) and primers 5′-*GATCGGATCC*GCTTCGCCCGAAACGAAA-3′ (forward; BamHI site is underlined) and 5′-*GATCGGTACC*TTGGTCATCCCAGATCTCTTCG-3′ (reverse; KpnI site is underlined). PCR product sizes were analyzed by gel electrophoresis, and the products were sequenced.

The *Tg*PI1 targeting construct was engineered by PCR amplifying 3.6 kb of *Tg*PI1 3′ flanking sequence with primers 5′-*GATCGGATCC*CAAAGGCATCTTTGCTTG-3′ (forward; BamHI site is underlined) and 5′-*GATCGAGCTC*TTTGCGTAAGTCTTGCCGTTG-3′ (reverse; SacI site is underlined) and cloning it downstream of the *dhfr*HXGPRT*dhfr* selectable marker (12). 5′ *Tg*PI1 sequence (2.5 kb) was amplified using primers 5′-GATGGTGTAGTGGTATCACGCCTGATTTGC-3′ (forward) and 5′-*AGATCTGGGCCCATAAGCTT*TTTACGACGGGTTAGCAC-3′ (reverse; underlined sequence indicates a link added to facilitate further fusion PCR) and joined to the *dhfr*HXGPRT*dhfr* cassette plus 3′ *Tg*PI1 sequences amplified using primers 5′-*AGCTTATGGGCCCAGATCTA*-3′ (forward; link sequence is underlined) and 5′-CACTCTAACGCGTTCACCCTAAATGGCC-3′ (reverse) by fusion PCR using the 5′ flanking region forward primer and *dhfr*HXGPRT*dhfr* plus 3′ flanking sequence reverse primer (underlined sequences indicate complementary nucleotides). RHΔHXGPRT strain parasite tachyzoites (10^7) (16) were directly transfected with 30 μg of the 8.1-kb fusion PCR product and selected in 25 μg/ml mycophenolic acid plus 50 μg/ml xanthine as previously described (16).

Surviving populations were screened for (i) loss of the *Tg*PI1 locus using primers 5′-*GATCGGATCC*CCCGTCGTAAAAATGGGAAAGAATCC-3′ (P1) (forward; BamHI site is underlined) and 5′-*GATCCCTAGG*TTGGTCATCCCAGATCTCTTCGG-3′ (P2) (reverse; AvrII site is underlined), (ii) presence of the HXGPRT selectable marker using primers 5′-GTCGGTTGACAAGTGTTCTGGCAGGC-3′ (P3) and 5′-CACTCTAACGCGTTCACCCTAAATGGCC-3′ (P4), and (iii) homologous recombination of HXGPRT into the *Tg*PI1 locus using primers P3 and 5′-

CTAGATGCAGTCTGCGGAGATAGCTCAT-3′ (P5). Positive populations were cloned by serial dilution in 96-well plates, and the isolated clones were screened using the same primers.

Fluorescent fusion proteins (for subcellular localization) and glutathione *S*-transferase (GST) fusion proteins (for functional complementation and purification) were engineered by amplifying *Tg*PI1α or *Tg*PI1β coding sequences using primers 5′-*GATCGGATCC*CCCGTCGTAAAAATGGGAAAGAATCC-3′ (forward) and 5′-*GATCCCTAGG*TTGGTCATCCCAGATCTCTTCGG-3′ (reverse) and cloning into plasmid *tub*mRFP, *tub*YFP, or *tub*GST (42), all of which harbor a *sag*CAT*sag* cassette; selected in 20 μM chloramphenicol; and cloned by limiting dilution.

For genomic hybridization, 5 μg DNA from parental RHΔHXGPRT parasites, *Tg*PI1 knockout mutants, and complemented clones was digested with EcoRI, separated on a 0.7% agarose gel, transferred to a Hybond N+ membrane (Amersham), and hybridized with digoxigenin probes (Roche) generated by PCR amplification of coding sequence primers 5′-CGCAGCAGGATGACGAATCTGA-3′ (forward) and P2 (see above) or 5′ flanking region primers 5′-CTCCTGTACCCTTTCGACTTCGTC-3′ (forward) and 5′-CGTTCCAGTTGTTCGTGCGGTGAAT-3′ (reverse).

For expression profiling, confluent monolayers of HFF grown in T25 flasks containing Dulbecco's modified Eagle medium supplemented with 20% medium 199 (Life Technologies) and 10% cosmic calf serum (HyClone) were inoculated with 5×10^5 RHΔHXGPRT or Δ*Tg*PI1 tachyzoites, and RNA was extracted after 36 h (RNeasy kit; Qiagen). The RNA was labeled using Ovation Amp v2 (NuGen) according to the manufacturer's instructions and hybridized to a custom T. gondii Affymetrix array (3). Gene expression levels were determined using robust multichip average (RMA) normalization.

Fluorescence microscopy. HFF grown on glass coverslips and infected with parasites were fixed for 20 min in 4% paraformaldehyde plus 0.02% glutaraldehyde, permeabilized for 15 min in 0.2% Triton X-100, washed several times in PBS, blocked for 30 to 60 min in 5% fetal bovine serum plus 3% bovine serum albumin (fraction V; Sigma), and incubated for 1 h with primary antibody (see above), followed by 1 h of incubation with Alexa 594- or Alexa 488-conjugated goat anti-mouse or goat anti-rabbit antiserum (Molecular Probes). The slides were mounted in Fluormount G (Southern Biotechnology) and imaged at ×100 using a Leica DM IRB microscope equipped with a high-resolution charge-coupled-device (CCD) camera (Orca-ER; Hamamatsu) and Openlab 5.5.1 software (Improvision).

***In vitro* assays**: parasite replication and differentiation.Intracellular T. gondii replication was assessed as previously described (19) by inoculating confluent HFF monolayers in six-well plates with 2×10^5 freshly purified tachyzoites. The monolayers were washed to remove extracellular parasites at 4 h, and replication was assessed at 12, 24, 30, and 36 h by fixation in 3.7% paraformaldehyde, staining with Giemsa stain, and scoring the number of intracellular parasites in 100 parasitophorous vacuoles selected at random. Each time point represents triplicate assays from two independent experiments; statistical analysis was based on the two-tailed Student's *t* test.

Parasite differentiation (17) was induced by inoculation of HFF monolayers in six-well plates, switching to minimal essential medium (MEM) containing 1 g/liter $NaHCO_3$ plus 50 mM Tricine (pH 8.1) at 4 h postinfection, and incubation at 37°C in 0.03% CO_2, replacing the medium every 6 to 8 h to maintain a constant alkaline pH. At 48 h, the cultures were fixed in 3.7% paraformaldehyde, permeabilized in 0.2% Triton X-100, blocked with 10% fetal bovine serum, and stained with 1:100 tetramethyl rhodamine isocyanate (TRITC)-conjugated Dolichos biflorus lectin (Sigma). One hundred randomly selected parasitophorous vacuoles were scored for a homogeneous cyst wall (average of three independent experiments).

Quantification of the parasite burden *in vivo*. Female 6- to 8-week-old BALB/c mice were infected by intraperitoneal injection of 10^3 parasite tachyzoites (RH wild type, Δ*Tg*PI1 mutant, or RHΔ*Tg*PI1 complemented with *Tg*PI1α or *Tg*PI1β). After sacrifice at 7 days postinfection, DNA was extracted from the liver, spleen, and brain (High Pure PCR Kit; Roche), and 100 ng of each sample was analyzed by quantitative PCR (25) using primers 5′-TCTTTAAAGCGTTCGTGGTC-3′ (forward) and 5′-GGAACTGCATCCGTTCATGAG-3′ (reverse) to determine the abundance of the multicopy T. gondii B1 gene (25) relative to a mouse β-actin control (forward, 5′-TCACCCACACTGTGCCCATCTACGA-3′; reverse, 5′-CAGCGGAACCGCTCATTGCCAATGG-3′). After 10 min of denaturation at 95°C, thermal cycling was carried out using 40 cycles of 1 min annealing/extension at 60°C, alternating with 15 s of denaturation at 95°C (Applied Biosystems 7500) and SYBR green detection. The $2^{-\Delta\Delta CT}$ method was used to calculate the relative parasite burdens in different tissues; analysis of serial dilutions of DNA from infected livers demonstrated similar amplification efficiencies for the *Tg*B1 target and mouse β-actin over a wide range of DNA concentrations.

Nucleotide sequence accession numbers. Updated *Tg*PI1 sequence information is available at ToxoDB.org (TgME49_008450) and in GenBank (accession numbers HM536610 [*Tg*PI1α], AF121778 [*Tg*PI1β], and HM536941 [genomic]).

Results and Discussion

Alternative splicing of a 72-nucleotide exon produced two *Tg*PI1 isoforms.Immunoblotting demonstrated two *Tg*PI1 isoforms in each of the three dominant lineages of T. gondii (Fig. 1A), as previously described for RH strain parasites (40, 44). Expression levels of the smaller isoform (designated *Tg*PI1β) were comparable in all strains tested, but the larger isoform (*Tg*PI1α) was reproducibly less abundant than *Tg*PI1β in strain RH, more abundant than *Tg*PI1β in the Pru strain, and comparable to *Tg*PI1β in VEG strain parasites.

To determine whether these two isoforms arise by posttranslational modification, extracellular T. gondii strain RH tachyzoites were labeled with ^{35}S-labeled amino acids for 15 min, and *Tg*PI1 was immunoprecipitated after 0 to 60 min of incubation in unlabeled medium. Both isoforms were observed at all time points (Fig. 1B), indicating that *Tg*PI1α and -β do not exhibit a precursor-product relationship, i.e., they are probably not attributable to proteolytic cleavage or other posttranslational modifications. Also, the altered migration is not due to differential N-linked glycosylation occurring cotranslationally in the endoplasmic reticulum, as the *Tg*PI1 deduced sequence is devoid of a consensus motif (NXS/T) for *N*-glycan addition.

To further investigate the relationship between *Tg*PI1α and -β, the isoforms were immunoaffinity purified from the supernatant of a heavily infected HFF monolayer shortly after parasite egress (when *Tg*PI1 is released from the disrupted vacuoles), and bands

obtained by gel electrophoresis were subjected to MALDI-TOF mass spectrometry (Fig. 1C). Intact protein masses were measured at 34.3 kDa for *Tg*PI1α and 31.5 kDa for *Tg*PI1β, and the molecular mass difference between the isoforms was estimated to be 2,775 ± 31 Da. A peptide mass fingerprint generated by tryptic digestion prior to MALDI-TOF revealed very similar spectra for *Tg*PI1α and *Tg*PI1β (Fig. 1D), differing only in the presence of a unique *m/z* peak at 1,652.7. This peak corresponds to a 15-amino-acid tryptic peptide (TQSSHQHDDAENGAR) that is unique to *Tg*PI1α, suggesting that *Tg*PI1α has a distinct genetically encoded segment.

To determine if the distinct segment is due to differential RNA splicing, we performed RT-PCR of total RNA from RH strain parasites using forward and reverse primers encompassing the full-length *Tg*PI1 coding sequence. This analysis yielded distinct transcripts of 887 nucleotides (nt) and 815 nt; the same bands were obtained by RT-PCR from an RH strain tachyzoite cDNA library, while a single band of 2,973 nt was obtained from genomic DNA (Fig. 1E). The relative abundances of the two *Tg*PI1 transcripts correlate with the relative abundances of the two protein isoforms in RH strain parasites (Fig. 1A, lane 1). Sequencing of the cloned products revealed that the larger species contains a 75-nt insertion predicted to encode 25 amino acids, including the extra peptide identified by mass spectrometry. This 25-amino-acid insert has a predicted mass of 2,752 Da, which is within the measurement range of the mass difference between *Tg*PI1α and *Tg*PI1β (2,775 ± 31 Da). Comparison with the TgME49_008450 genomic locus (ToxoDB.org) identified the extra sequence as a distinct exon, defining alternatively spliced mRNAs of 8 versus 9 exons (Fig. 1F); several expressed sequence tags (ESTs) validate each of these transcripts and confirm the alternative splicing of *Tg*PI1. All predicted *Tg*PI1 introns begin with GT and end with AG, in agreement with the consensus for other eukaryotes (including T. gondii), and sequence upstream of the first ATG corresponds to the consensus for translational initiation in T. gondii (AAAATG). The first 24 amino acids (most of the first exon) are predicted to comprise a secretory signal sequence. Exons 2, 4, 7, and 9 each encode a Kazal domain (asterisks in Fig. 1F), while exons 1, 3, 5, 6, and 8 encode linkers between the Kazal domains (44); the alternatively spliced exon expands the linker between the third and fourth Kazal domains in *Tg*PI1α. This modular structure is consistent with the repeated duplications typical of multidomain Kazal inhibitor evolution (29). The identification of alternative splicing of the *Tg*PI1 gene adds to the growing list of examples of transcript (and protein) diversity generated by splicing in T. gondii (14, 16, 30, 53).

Targeted deletion and complementation of the *Tg*PI1 locus. To investigate the function of *Tg*PI1, the genomic locus was deleted by homologous replacement using HXGPRT as a positive selectable marker in the RHΔHXGPRT background (16). Figure 2A displays the *Tg*PI1 genomic locus and the targeting construct used to generate Δ*Tg*PI1 knockout parasites. Transfected parasites were inoculated into HFF in six wells of a 24-well plate, selected in mycophenolic acid, and screened by PCR upon host cell lysis (~5 to 7 days posttransfection) to identify wells containing candidate knockouts. Individual parasites from two positive wells were cloned by limiting dilution in 96-well plates and rescreened by PCR (Fig. 2B) to identify clones lacking the *Tg*PI1 gene (Fig. 2A, P1-P2) in which the selectable marker had integrated at the endogenous

*Tg*PI1 locus (P3-P4 and P3-P5). Gene replacement was confirmed by Southern blotting: a probe amplified from genomic DNA showed complete loss of *Tg*PI1 coding sequence (Fig. 2C, left, compare lane 1 with lanes 2 and 3), and a flanking sequence probe demonstrated the expected 800-nt decrease in size from the 12.3-kb EcoRI fragment encompassing *Tg*PI1 (Fig. 2C, right, lane 1 versus lanes 2 and 3).

For genetic complementation, *Tg*PI1 knockout (Δ*Tg*PI1) parasites were transfected with plasmids engineered to express cDNA encoding *Tg*PI1α or *Tg*PI1β fused to GST, to facilitate future pull-down studies, flanked by a β-tubulin promoter and a dihydrofolate reductase-thymidylate synthase (DHFR-TS) 3′ untranslated region. A chloramphenicol acetyltransferase (CAT) selectable marker was incorporated into the complementation plasmid, and Southern blotting of genomic DNA from clonal parasite transfectants revealed the expected 5.2-kb EcoRI fragment containing the *Tg*PI1 transgene; additional bands corresponded to integration events fragmenting the *Tg*PI1 transgene (Fig. 2C, left, lanes 4 and 5). Western blotting using rabbit anti-*Tg*PI1 (Fig. 2D) or anti-GST (not shown) demonstrated loss of *Tg*PI1 in Δ*Tg*PI1 parasites and expression of a single *Tg*PI1-GST protein of the expected size in *Tg*PI1α or *Tg*PI1β transgenic parasite lysates (smaller bands may be attributable to proteolytic cleavage).

Targeted deletion of a gene family member in T. gondii can lead to upregulation of another member of the gene family (46). To determine whether deletion of *Tg*PI1 resulted in compensatory upregulation of other T. gondii genes, including those encoding other serine protease inhibitors, we performed genome-wide expression profiling using a custom T. gondii Affymetrix microarray (Toxodb.org) (Fig. 2E). Interpro motif searches identified eight putative protease inhibitors in the T. gondii genome: six Kazal-type inhibitors (TgME49_008450 [*Tg*PI1], TgME49_008430 [*Tg*PI2], TgME49_083470, TgME49_059890, TgME49_024080, and TgME49_066610) and two serpins (TgME49_017430 and TgME49_046130). Only four of them exhibited steady-state transcript levels above background (*Tg*PI1, *Tg*PI2, and the two serpins). As expected, *Tg*PI1 transcripts were reduced to background levels (>200-fold decrease) in the Δ*Tg*PI1 mutants. Steady-state transcript levels for *Tg*PI2 were ~10-fold lower than for *Tg*PI1 in both control parasites and the Δ*Tg*PI1 knockout. This finding confirms earlier studies showing low but detectable expression of *Tg*PI2 protein in tachyzoites (39), and it demonstrates a lack of compensation by *Tg*PI2 in the Δ*Tg*PI1 knockout. Similarly, no compensatory expression or other changes were observed in other protease inhibitor genes. These observations were confirmed by quantitative PCR (not shown).

***Tg*PI1α and *Tg*PI1β are secreted into the parasitophorous vacuole and are also transferred to the host cell cytoplasm.** Indirect immunofluorescence using rabbit antisera to recombinant *Tg*PI1 showed expression of *Tg*PI1 in parental RHΔHXGPRT parasites (Fig. 3A), loss of expression in Δ*Tg*PI1 (Fig. 3B), and restoration in both Δ*Tg*PI1 plus PI1α-GST and Δ*Tg*PI1 plus PI1β-GST transgenics (Fig. 3C and D). *Tg*PI1 is secreted via dense granules into the parasitophorous vacuole (45) (Fig. 3A), and expression of *Tg*PI1α or *Tg*PI1β in Δ*Tg*PI1 knockout mutants demonstrated that both isoforms were also secreted into the parasitophorous vacuole (Fig. 3C and D). Interestingly, *Tg*PI1 was also observed in the cytoplasm of a subset (57% ± 5% in three independent replicates) of infected host cells, along with another dense-granule protein, GRA1 (Fig. 3E). In contrast, a P30-OVA transgene (43) expressed in the same cells was not seen in the host cell cytoplasm despite being abundantly present in the

parasitophorous vacuole (Fig. 3F). P30-OVA, which consists of the P30 (SAG1) signal sequence fused to the model antigen ovalbumin, serves as a default secretory marker lacking specific targeting signals. Moreover, *Tg*PI1 localization to the host cytoplasm was observed in a majority of infected host cells, including those containing small, as well as large, parasitophorous vacuoles, although fluorescence is usually stronger in the latter, presumably due to the presence of more parasites secreting *Tg*PI1. The fact that *Tg*PI1 and GRA1 were seen in the cytoplasm of host cells containing a range of parasitophorous vacuoles suggests that cytoplasmic transfer was not a result of vacuolar permeabilization resulting from imminent parasite egress. For further validation, we transfected Δ*Tg*PI1 parasites with plasmids encoding *Tg*PI1α fused to monomeric red fluorescent protein (mRFP) or *Tg*PI1β fused to yellow fluorescent protein (YFP). Both of these *Tg*PI1–fluorescent-protein fusions were observed in the cytoplasm of live infected HFF (Fig. 3G and H), ruling out the possibility that transfer of *Tg*PI1 to the host cytoplasm occurred during fixation. These findings suggest that *Tg*PI1 has access to potential targets in the host cytoplasm, thus opening the possibility that *Tg*PI1 suppresses host proteases during intracellular growth.

Δ*Tg*PI1 tachyzoites exhibit normal replication but enhanced differentiation *in vitro*. To determine if *Tg*PI1 influences parasite replication, confluent HFF monolayers were inoculated with an equivalent number of wild-type RH strain tachyzoites, RHΔHXGPRT parasites, Δ*Tg*PI1 knockouts, or clonal parasite lines complemented with *Tg*PI1α-GST or *Tg*PI1β-GST. ΔHXGPRT parasites display a slight growth defect (Fig. 4A) (a doubling time of 9.2 ± 0.9 h for RHΔHXGPRT versus 7.1 ± 0.6 h for wild-type RH), as previously described (9). However, Δ*Tg*PI1 knockout parasites, which express HXGPRT, displayed a doubling time (~7.8 ± 0.4 h) that was indistinguishable from that of wild-type RH. Strains expressing *Tg*PI1α and *Tg*PI1β also exhibited doubling times similar to that of the wild type (~6.7 and 7.7 h, respectively). Thus, *Tg*PI1 expression appears to have no significant impact on T. gondii tachyzoite replication *in vitro*. Since RHΔHXGPRT has different growth properties due to the lack of HXGPRT expression, the wild-type RH strain is used here as the reference strain.

T. gondii strain RH does not form mature bradyzoite cysts in mice but can be induced to differentiate *in vitro* under stress conditions, such as exposure to alkaline pH (4, 5, 17, 18, 52, 54, 57). Bradyzoite-specific antigens are detected as early as 12 to 24 h postinduction (P. H. Davis, unpublished data), and cyst wall development can be visualized by staining with D. biflorus lectin (6). To test if *Tg*PI1 plays a role in stage differentiation, confluent monolayers of HFF were infected with wild-type RH, the ΔHXGPRT or Δ*Tg*PI1 knockout mutant, and complemented parasite lines and assayed for differentiation after 48 h of incubation at pH 8.1 (Fig. 4B). Δ*Tg*PI1 knockout parasites showed a 64-fold upregulation of the bradyzoite-specific enolase isozyme ENO1 (Fig. 4B) (27) relative to wild-type T. gondii. Knockout parasites also showed a similar hyperinduction of other bradyzoite stage-specific markers, including P18/SAG4.2, BAG1, and LDH2 (upregulated 13-, 25-, and 30-fold, respectively).

Low levels of Dolichos staining were observed in alkali-treated T. gondii strain RH cultures (Fig. 4C, left), perhaps associated with the intravacuolar membrane network (34), but only ~8% of these vacuoles showed evidence of bradyzoite cyst differentiation, including (i) high levels of Dolichos lectin staining on the vacuolar surface, (ii) reduced replication (2 to 8 parasites within the vacuole versus 16 to 32 in tachyzoite-containing vacuoles), (iii) rounded parasite morphology lacking the “rosette” organization typical of tachyzoites, and (iv) rounded, cyst-like vacuoles

(Fig. 4C). In contrast, 74% of vacuoles containing Δ*Tg*PI1 knockouts were strongly Dolichos positive, and complementation with either *Tg*PI1α or *Tg*PI1β substantially reversed the differentiation phenotype (Fig. 4B). Thus, deletion of *Tg*PI1 enhances bradyzoite differentiation of RH strain parasites *in vitro*. While other T. gondii mutants are also prone to enhanced bradyzoite differentiation (cf. the ΔHXGPRT mutant in Fig. 4B), the Δ*Tg*PI1 effect is particularly profound. It is possible that *Tg*PI1 inhibits proteases involved in bradyzoite cyst formation, as the cyst wall contains chitin (6) and there is ample precedent for proteolytic regulation of chitin in other systems (7, 13, 37).

Deletion of *Tg*PI1 increases the parasite tissue burden in infected mice. To assess the importance of *Tg*PI1 *in vivo*, BALB/c mice were inoculated with freshly harvested tachyzoites by intraperitoneal injection, and the liver, spleen, and brain were harvested from euthanized animals during the acute phase of infection 7 days postinoculation. The parasite tissue burden was measured by quantitative PCR. Infection with RH strain parasites develops rapidly and is typically fatal on approximately day 8 postinoculation, which is prior to the initiation of the chronic phase of infection (days 10 to 12 for cystogenic strains [15]). As shown in Fig. 4D, Δ*Tg*PI1 tachyzoites reproducibly displayed significantly higher parasite burdens than the RH strain in all tissues (three independent experiments). Complementation with either *Tg*PI1α or *Tg*PI1β reduced the parasite burden to the level observed in wild-type controls in the spleen. A similar trend was seen in the liver, although Δ*Tg*PI1β did not fully reverse the elevated parasite burden phenotype. Neither *Tg*PI1α nor *Tg*PI1β restored the normal parasite burden in the brain, which is low and highly variable, thus possibly explaining the apparent lack of complementation. Alternatively, it is possible that *Tg*PI1α and *Tg*PI1β each target different proteases in the brain, and therefore, complementation with both isoforms would be necessary to restore normal infection levels.

Most other dense-granule protein mutants that have been characterized to date exhibit either no phenotype (GRA5) (27) or reduced virulence (GRA2, GRA3, and GRA6) (12, 35, 36). In contrast, deletion of *Tg*PI1 appears to enhance the parasite burden during acute tachyzoite infection of mice. This phenotype is reminiscent of a recently reported type II strain GRA15 knockout mutant, which replicated to greater levels in mice than wild-type parasites (48). GRA15 is associated with the PV and appears to have access to the cytoplasm of infected host cells, where it activates nuclear translocation of NF-κB in a parasite strain-dependent manner, resulting in upregulation of several genes, including the proinflammatory cytokine interleukin 12 (IL-12). Rapid production of IL-12 during early infection with type II parasites induces gamma interferon (IFN-γ), which suppresses parasite growth (38). Conversely, deletion of GRA15 delays production of IL-12 and IFN-γ, thus permitting rapid growth and a higher parasite burden *in vivo*. While *Tg*PI1 ablation also leads to a higher parasite burden *in vivo*, precisely how *Tg*PI1 affects parasite growth in mice remains to be determined. Although higher levels of *Tg*PI1 expression, especially *Tg*PI1α, in the Pru strain correlates with the slower growth and reduced virulence of this type II strain, strain-specific virulence genes have not been mapped to chromosome Ib, where *Tg*PI1 is encoded. Future studies focused on the identification of proteases targeted by *Tg*PI1 during infection should provide further insight into how *Tg*PI1 influences T. gondii differentiation and growth *in vivo*.

Acknowledgements

We thank Michael Grigg, Karen Ehrenman, and members of the Carruthers, Hunter, and Roos laboratories for critical comments on the manuscript.

This work was supported by research grants AI28724 (D.S.R.), AI077268 and RR16469 (P.H.D.), AI046675 (V.B.C.), and AI42334 (C.A.H.) from the NIH.

References

Armstrong PB. 2006. Proteases and protease inhibitors: a balance of activities in host-pathogen interaction. Immunobiology 211:263–281.

Bahl A, et al. 2010. A novel multifunctional oligonucleotide microarray for *Toxoplasma gondii*. BMC Genomics 11:603.

Beiting DP, Roos DS. 2011. A systems biological view of intracellular pathogens. Immunol. Rev. 240 :117–128.

Bohne W, Heesemann J, Gross U. 1993. Induction of bradyzoite-specific *Toxoplasma gondii* antigens in gamma interferon-treated mouse macrophages. Infect. Immun. 61:1141–1145.

Bohne W, Heesemann J, Gross U. 1994. Reduced replication of Toxo- plasma gondii is necessary for induction of bradyzoite-specific antigens: a possible role for nitric oxide in triggering stage conversion. Infect. Immun. 62:1761–1767.

Boothroyd JC, et al. 1997. Genetic and biochemical analysis of development in *Toxoplasma gondii*. Philos. Trans. R. Soc. Lond. B 352 :1347–1354.

Broehan G, Zimoch L, Wessels A, Ertas B, Merzendorfer H. 2007. A chymotrypsin-like serine protease interacts with the chitin synthase from the midgut of the tobacco hornworm. J. Exp. Biol. 210:3636–3643.

Bruno S, et al. 2004. Identification and characterization of serine proteinase inhibitors from *Neospora caninum*. Mol. Biochem. Parasitol. 136:101–107.

Chaudhary K, et al. 2004. Purine salvage pathways in the apicomplexan parasite *Toxoplasma gondii*. J. Biol. Chem. 279:31221–313227.

Chen F, Mackey AJ, Stoeckert CJ, Jr, Roos DS. 2006. OrthoMCL-DB: querying a comprehensive multi-species collection of ortholog groups. Nucleic Acids Res. 34:D363–D368.

Cohen SL, Chait BT. 1997. Mass spectrometry of whole proteins eluted from sodium dodecyl sulfate-polyacrylamide gel electrophoresis gels. Anal. Biochem. 247:257–267.

Craver MP, Knoll LJ. 2007. Increased efficiency of homologous recombination in *Toxoplasma gondii* dense granule protein 3 demonstrates that GRA3 is not necessary in cell culture but does contribute to virulence. Mol. Biochem. Parasitol. 153 :149–157.

Danielli A, et al. 2000. A modular chitin-binding protease associated with hemocytes and hemolymph in the mosquito *Anopheles gambiae*. Proc. Natl. Acad. Sci. U. S. A. 97:7136–7141.

Delbac F, et al. 2001. *Toxoplasma gondii* myosins B/C: one gene, two tails, two localizations, and a role in parasite division. J. Cell Biol. 155 :613–623.

Di Cristina M, et al. 2008. Temporal and spatial distribution of *Toxoplasma gondii* differentiation into bradyzoites and tissue cyst formation in vivo. Infect. Immun. 76:3491–3501.

Donald RGK, Carter D, Ullman B, Roos DS. 1996. Insertional tagging, cloning, and expression of the *Toxoplasma gondii* hypoxanthine-xanthine-guanine phosphoribosyltrans gene. Use as a selectable marker for stable transformation. J. Biol. Chem. 271:14010–14019.

Dzierszinski F, Nishi M, Ouko L, Roos DS. 2004. Dynamics of *Toxoplasma gondii* differentiation. Eukaryot. Cell 3 :992–1003.

Ferreira da Silva MF, Barbosa HS, Gross U, Lüder CG. 2008. Stress- related and spontaneous stage differentiation of *Toxoplasma gondii*. Mol. Biosyst. 4 :824–834.

Fichera ME, Bhopale MK, Roos DS. 1995. *In vitro* assays elucidate the peculiar kinetics of clindamycin action against *Toxoplasma gondii*. Anti- microb. Agents Chemother. 39 :1530–1537.

Goldberg B, Stricker RB. 1996. HIV protease and the pathogenesis of AIDS. Res. Virol. 147:375–379.

Harrison LM, et al. 2002. Molecular characterization of *Ancylostoma* inhibitors of coagulation factor Xa. Hookworm anticoagulant activity in vitro predicts parasite blood feeding in vivo. J. Biol. Chem. 277 :6223–6229.

Hemmi H, et al. 2005. Structural and functional study of an *Anemonia elastase* inhibitor, a "nonclassical" Kazal-type inhibitor from *Anemonia sulcata*. Biochemistry 44:9626–9636.

Howe DK, Sibley LD. 1995. *Toxoplasma gondii* comprises three clonal lineages: correlation of parasite genotype with human disease. J. Infect. Dis. 172:1561–1566.

Ingmer H, Brøndsted L. 2009. Proteases in bacterial pathogenesis. Res. Microbiol. 160:704–710.

Jauregui Higgins LHJ, Zarlenga D, Dubey JP, Lunney JK. 2001. Development of a real-time PCR assay for detection of *Toxoplasma gondii* in pig and mouse tissues. J. Clin. Microbiol. 39:2065–2071.

Joiner KA, Roos DS. 2002. Secretory traffic in *Toxoplasma gondii*: less is more. J. Cell Biol. 157:557–563.

Kibe MK, et al. 2005. Transcriptional regulation of two stage-specifically expressed genes in the protozoan parasite *Toxoplasma gondii* . Nucleic Acids Res. 33:1722–1736.

Krowarsch D, Cierpicki T, Jelen F, Otlewski J. 2003. Canonical protein inhibitors of serine proteases. Cell. Mol. Life Sci. 60:2427–2444.

Laskowski M, Jr, Kato I, Kohr WJ, March CJ, Bogard WC. 1980. Evolution of the family of serine proteinase inhibitors homologous to pancreatic secretory trypsin inhibitor (Kazal), p 123–128. In Peeters H (ed), Protides of biological fluids. Pergamon, Oxford, United Kingdom.

Ling Y, Li Z, Miranda K, Oldfield E, Moreno SNJ. 2007. The farnesyldiphosphate/geranylgeranyl-diphosphate synthase of *Toxoplasma gondii* is a bifunctional enzyme and a molecular target of bisphosphonates. J. Biol. Chem. 282:30804–30806.

Macen JL, Upton C, Nation N, McFadden G. 1993. SERP-1, a serine proteinase inhibitor encoded by myxoma virus, is a secreted glycoprotein that interferes with inflammation. Virology 195:348–383.

Martzen MR, Geise GL, Hogan BJ, Peanasky AJ. 1985. *Ascaris sum*: localization by immunochemical and fluorescent probes of host proteases and parasite proteinase inhibitors in cross-sections. Exp. Parasitol. 60:139–149.

McKerrow JH, Sun E, Rosenthal PJ, Bouvier J. 1993. The proteases and pathogenicity of parasitic protozoa. Annu. Rev. Microbiol. 47:821–853.

Mercier C, Adjogble KDZ, Däubener W, Cesbron-Delauw MF. 2005. Dense granules: are they key organelles to help understand the parasitophorous vacuole of all apicomplexa parasites? Int. J. Parasitol. 35:829–849.

Mercier C, Howe DK, Mordue D, Lingnau M, Sibley LD. 1998. Targeted disruption of the GRA2 locus in *Toxoplasma gondii* decreases acute virulence in mice. Infect. Immun. 66: 4176–4182.

Mercier C, et al. 2001. Lack of expression of the dense granule protein GRA5 does not affect the development of *Toxoplasma* tachyzoites. Mol. Biochem. Parasitol. 116:247–251.

Miyamoto K, et al. 2002. Molecular analysis of the gene encoding a novel chitin-binding protease from Alteromonas sp. strain O-7 and its role in the chitinolytic system. J. Bacteriol. 184:1865–1872.
Mordue DG, Monroy F, LaRegina M, Dinarello CA, Sibley LD. 2001. Acute toxoplasmosis leads to lethal overproduction of Th1 cytokines. J. Immunol. 167:4574–4584.
Morris MT, Carruthers VB. 2003. Identification and partial character- ization of a second Kazal inhibitor in *Toxoplasma gondii*. Mol. Biochem. Parasitol. 128:119–122.
Morris MT, Coppin A, Tomavo S, Carruthers VB. 2002. Functional analysis of *Toxoplasma gondii* protease inhibitor 1. J. Biol. Chem. 277:45259–45266.
Morris MT, Cheng W, Zhou XW, Brydges SD, Carruthers VB. 2004. *Neospora caninum* expresses an unusual single-domain Kazal protease inhibitor that is discharged into the parasitophorous vacuole. Int. J. Parasitol. 34:693–701.
Nishi M, Hu K, Murray JM, Roos DS. 2008. Organellar dynamics during the cell cycle of *Toxoplasma gondii*. J. Cell Sci. 121:1559–1568.
Pepper M, Dzierszinski F, Crawford A, Hunter CA, Roos D. 2004. Development of a system to study CD4-T-Cell responses to transgenic ovalbumin-expressing *Toxoplasma gondii* during toxoplasmosis. Infect. Immun. 72:7240–7246.
Pszenny V, et al. 2000. Molecular cloning, sequencing and expression of a serine proteinase inhibitor gene from *Toxoplasma gondii*. Mol. Biochem. Parasitol. 107:241–249.
Pszenny V, et al. 2002. Subcellular localization and post-secretory targeting of Tg PI, a serine proteinase inhibitor from *Toxoplasma gondii*. Mol. Biochem. Parasitol. 121:283–286.
Que X, et al. 2007. Cathepsin Cs are key for the intracellular survival of the protozoan parasite, *Toxoplasma gondii*. J. Biol. Chem. 282:4994–5003.
Roos DS, Donald RG, Morrissette NS, Moulton ALC. 1994. Molecular tools for genetic dissection of the protozoan parasite *Toxoplasma gondii*. Methods Cell. Biol. 45:27–63.
Rosowski EE, et al. 2011. Strain-specific activation of the NF-kappaB pathway by GRA15, a novel *Toxoplasma gondii* dense granule protein. J. Exp. Med. 208 :195–212.
Shepherd JC, Aitken A, McManus DP. 1991. A protein secreted in vivo by *Echinococcus granulosus* inhibits elastase activity and neutrophil chemotaxis. Mol. Biochem. Parasitol. 44:81–90.
Shevchenko A, Wilm M, Vorm O, Mann M. 1996. Mass spectrometric sequencing of proteins silver-stained polyacrylamide gels. Anal. Chem. 68:850–858.
Stassens P, et al. 1996. Anticoagulant repertoire of the hookworm *Ancylostoma caninum*. Proc. Natl. Acad. Sci. U. S. A. 93:2149–2154.
Tomavo S, Boothroyd JC. 1995. Interconnection between organellar functions, development and drug resistance in the protozoan parasite *Toxoplasma gondii*. Int. J. Parasitol. 25:1293–1299.
Toursel C, Dzierszinski F, Bernigaud A, Mortuaire M, Tomavo S. 2000. Molecular cloning, organellar targeting and developmental expression of mitochondrial chaperone HSP60 in *Toxoplasma gondii*. Mol. Biochem.Parasitol. 111:319–332.
Weiss LM, LaPlace D, Tanowitz HB, Wittner M. 1992. Identification of *Toxoplasma gondii* bradyzoite-specific monoclonal antibodies. J. Infect. Dis. 166:213–215.
Zang X, Maizels RM. 2001. Serine proteinase inhibitors from nematodes and the arms race between host and pathogen. Trends Biochem. Sci. 26:191–197.
Zang X, Yazdanbakhsh M, Jiang H, Kanost MR, Maizels RM. 1999. A novel serpin expressed by blood-borne microfilariae of the parasitic nematode *Brugia malayi* inhibits human neutrophil serine proteinases. Blood 94:1418–1428.

Zhang YW, Halonen SK, Ma YF, Wittner M, Weiss LM. 2001. Initial characterization of CST1, a *Toxoplasma gondii* cyst wall glycoprotein. Infect. Immun. 69:501–507.

Figures

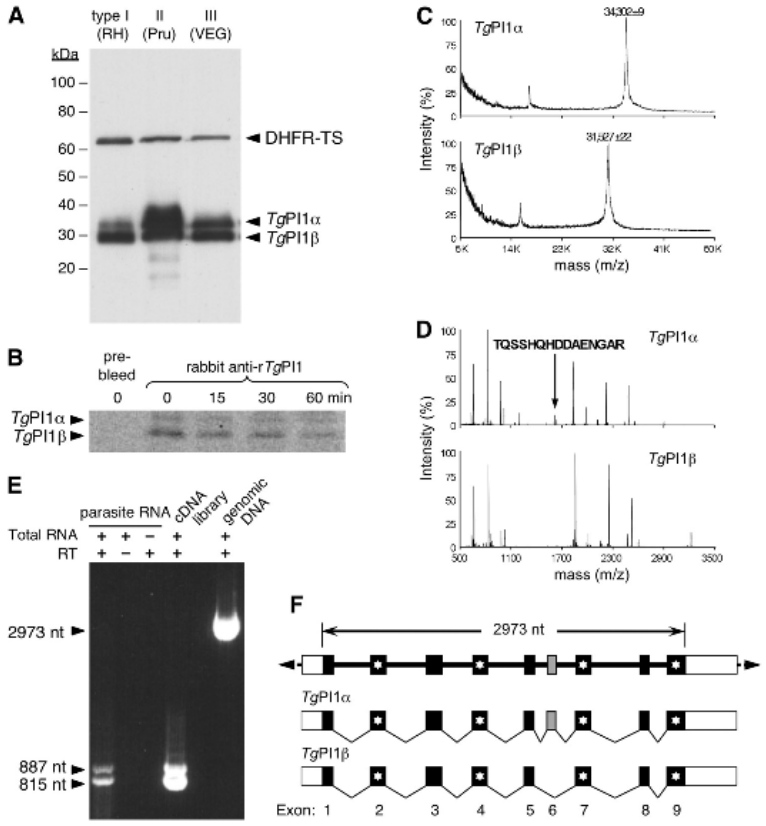

Fig 1

*Tg*PI1α and *Tg*PI1β are mRNA splice variants. (A) Western blotting with anti-*Tg*PI1 revealed two isoforms (*Tg*PI1α and *Tg*PI1β) in T. gondii strains RH (type I), Pru (type II), and VEG (type III). Each lane contained 10^6 parasite equivalents. (B) Pulse-chase labeling of intracellular RH strain tachyzoites with ^{35}S-labeled amino acids showed no evidence of posttranslational modification. (C) MALDI-TOF analysis of the two intact isoforms revealed an exact molecular mass difference of 2,775 Da (the average of three independent replicates). (D) MALDI-TOF analysis of tryptic fragments revealed a peak at *m/z* 1,652.7 specific to *Tg*PI1α (arrow). (E) RT-PCR showed reverse transcriptase (RT)-dependent amplification of 887- and 815-nt bands in samples containing total tachyzoite RNA (lane 1) or a cDNA library (lane 4); amplification from genomic DNA yielded a 2,973-nt band (lane 5). (F) Schematic representation of the two alternatively spliced variants of *Tg*PI1. The boxes represent exons (open, untranslated; filled, coding; gray, alternatively spliced exon 6). The white stars indicate predicted Kazal domains.

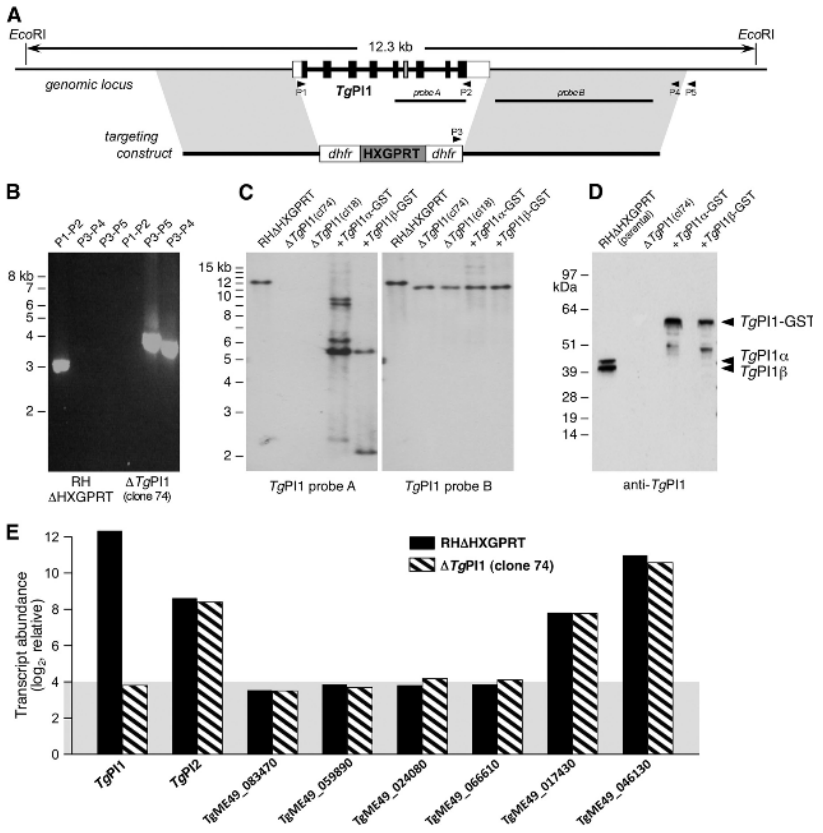

Fig 2

Targeted deletion of the *Tg*PI1 locus. (A) (Top) Scale diagram of the 12.3-kb EcoR I fragment spanning the *Tg*PI1 genomic locus. The boxes represent all nine *Tg*PI1 exons (open, untranslated; filled, coding; gray, alternatively spliced exon in *Tg*PI1α). (Bottom) *dhfr*HXGPRT*dhfr* targeting construct used for gene disruption. The shaded parallelograms denote identity to sequences flanking *Tg*PI1 (2.5 kb upstream and 3.6 kb downstream). Arrowheads, primers for PCR screening; bars, probes for Southern hybridization. (B) PCR of the *Tg*PI1 locus in RHΔHXGPRT parental parasites and one (of several) Δ*Tg*PI1 mutant clones. The *Tg*PI1 locus is present in parental parasites, but not the mutant (P1-P2) or the targeting construct integrated at the genomic locus (P3-P5 and P3-P4). Panel A shows the primer positions. (C) Southern blot illustrating deletion of the genomic *Tg*PI1 locus in two Δ*Tg*PI1 clones and integration of *Tg*PI1α or *Tg*PI1β transgenes at heterologous sites in complemented lines (panel A shows the probes). (D) Western blot with rabbit anti-*Tg*PI1 illustrating expression of both *Tg*PI1α and *Tg*PI1β isoforms in parental parasites, loss in Δ*Tg*PI1 mutants, and expression of *Tg*PI1α-GST or *Tg*PI1β-GST fusion proteins in parasites expressing complementation constructs. (E) Microarray analysis of steady-state transcript abundance ($\log_2$ values) for *Tg*PI1 and other protease inhibitor genes in parental RHΔHXGPRT and Δ*Tg*PI1 parasites. The gray shading indicates background expression levels.

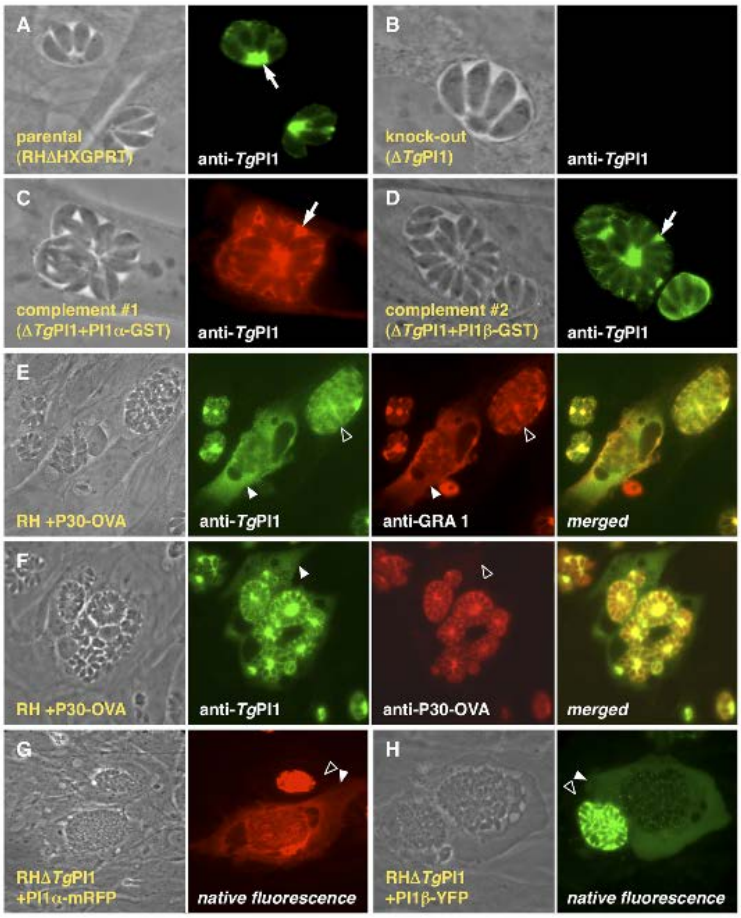

Fig 3

*Tg*PI1α and *Tg*PI1β are secreted into the parasitophorous vacuole and the host cell cytoplasm. (A to D) Immunofluorescence with anti-*Tg*PI1 demonstrates staining of the parasitophorous vacuole in parental parasites, no staining in Δ*Tg*PI1 mutants, and restoration in knockouts complemented with either *Tg*PI1α-GST or *Tg*PI1β-GST. The arrows indicate vacuoles containing parasites expressing *Tg*PI1. (E and F) Colocalization of *Tg*PI1 and GRA1, but not P30-OVA, in the cytoplasm of host cells infected with parasites expressing a P30-OVA transgene. (G and H) Identification of *Tg*PI1α and *Tg*PI1β in the host cell cytoplasm using fluorescent protein reporters (in live cell cultures). The closed arrowheads indicate staining of the parasitophorous vacuole and cytoplasm of host cells. The open arrowheads show vacuoles with no evidence of *Tg*PI1 staining in the cytoplasm of host cells.

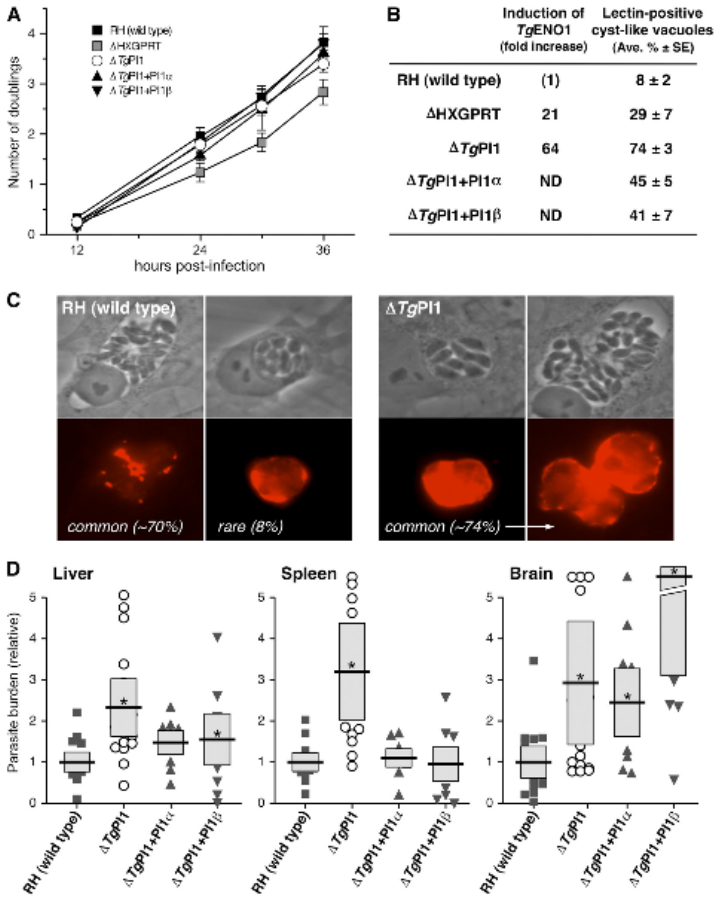

Fig 4

Phenotypic effects of Δ*Tg*PI1 *in vitro* and *in vivo*. (A) Δ*Tg*PI1 mutants are identical to wild-type parasites with respect to proliferation *in vitro*, as assessed by scoring parasite replication at various times postinfection (the average $\log_2$[parasite number] for 100 intracellular vacuoles, in triplicate). Doubling times were ~6.7 to 7.8 h for wild-type RH, Δ*Tg*PI1 knockout mutants, and Δ*Tg*PI1 plus PI1α- and Δ*Tg*PI1 plus *Tg*PI1β-complemented lines, in contrast to the slightly crippled replication rate of RHΔHXGPRT (9.2 ± 0.9 h). The error bars indicate standard deviations (SD). (B) Enhanced *in vitro* differentiation of Δ*Tg*PI1. Treatment for 48 h at pH 8.1 induced expression of the bradyzoite differentiation marker ENO1 (measured by quantitative PCR) and surface staining with D. biflorus lectin. Differentiation of Δ*Tg*PI1 was more extensive than that of ΔHXGPRT and much more than was observed in wild-type parasites. Partial complementation was observed in both Δ*Tg*PI1 plus PI1α and Δ*Tg*PI1 plus PI1β; ND, not determined. Ave., average; SE, standard error. (C) Morphology of alkaline-treated parasite cultures stained with fluorescent Dolichos lectin. Weak intravacuolar staining was observed for ~70% of wild-type parasites (left), while ~8% displayed strong Dolichos staining of the vacuolar surface and rounded bradyzoite cyst-like morphology (the remaining vacuoles were unstained). Approximately 70% of Δ*Tg*PI1 vacuoles displayed bradyzoite morphology, even when extensive replication was observed (far right). (D) Enhanced virulence of Δ*Tg*PI1 *in vivo*. Female BALB/c mice inoculated with 10^3 tachyzoites showed higher tissue burdens of Δ*Tg*PI1

than of the wild-type in the liver, spleen, and brain at day 7 postinfection. Full or partial complementation was observed for both Δ*Tg*PI1 plus PI1α and Δ*Tg*PI1 plus *Tg*PI1β in the liver and spleen, but not the brain (the bars show means ± SD for 2 or 3 experiments involving 2 to 5 mice per sample). The asterisks indicate a *P* value of ≤0.05 relative to RH (wild type). See the text for further discussion.